Available online at www.sciencedirect.com
ScienceDirect
Journal of Photochemistry and Photobiology A: Chemistry 187 (2007) 167–176
Journal of Photochemistry and Photobiology A:Chemistry
www.elsevier.com/locate/jphotochem

Photocatalytic degradation of Michler's Ethyl Ketone in titanium dioxide dispersions under UV irradiation

Chung-Shin Lu [a,*], Chiing-Chang Chen [a], Fu-Der Mai [b], Yi-Chin Wu [b]

[a] Department of General Education, National Taichung Nursing College, Taichung 403, Taiwan, ROC
[b] Department of Applied Chemistry, Chung-Shan Medical University, Taichung 403, Taiwan, ROC

Received 25 May 2006; received in revised form 21 August 2006; accepted 11 October 2006
Available online 10 November 2006

Abstract

Michler's Ethyl Ketone (MEK) can be degraded photocatalytically under UV irradiation in aqueous dispersions. In the presence of both UV light illumination and TiO_2 catalyst, MEK was more effectively degraded than with either UV or TiO_2 alone. Results obtained show rapid and complete oxidation of MEK after 20-h, and more than 94% of the MEK was mineralized after a 48-h exposure to UV-365 nm irradiation. To obtain a better understanding on the mechanistic details of this TiO_2-assisted photodegradation of the MEK with UV irradiation, 19 intermediates of the process were separated, identified, and characterized by HPLC-ESI-MS and GC–MS techniques in this study. The analytical results indicated that the photocatalytic degradation of MEK yielded intermediates such as *N*-hydroxyethylated species, *N*-de-ethylated compounds, aminobenzoic acid derivatives, aminobenzene derivatives, and aliphatic products. The possible degradation pathways were proposed and discussed on the basis of the evidence of oxidative intermediate formation. The reaction mechanisms of TiO_2/UV proposed in this research should prove useful in future efforts to breakdown the organic compounds in wastewater.

Keywords: Michler's Ethyl Ketone; Photodegradation; TiO_2; Photocatalytic

1. Introduction

4-(*N*,*N*-Diethylamino)-4′-(*N*′,*N*′-diethylamino)benzophenone (Michler's Ethyl Ketone, MEK) is used in certain screen printing inks because of its ability to extend the durability of the coating. It is commonly used in the manufacture of road signs and signs mounted on commercial vehicles. MEK can also be used in systems printing carton-board used for food packaging. It acts as a curing agent which hardens the ink when it is exposed to ultraviolet light during the printing process [1]. The genotoxicity of paper and paperboard extracts and the compounds found in them has been investigated by *Rec*-assay and comet assay. The results showed that most recycled paper products containing chemicals like Michler's Ketone and Michler's Ethyl Ketone possess genotoxicity [2]. The massive use of MEK has well-known noxious consequences on the human environment. Therefore, finding a method of treating MEK-containing wastewater is crucial.

To de-pollute the organic compounds in wastewater, a number of methods – including adsorption on various adsorbents [3–5], chemical oxidation [6], microbial action (biodegradation) [7,8], photolysis [9–17] and photocatalysis [18–26] – have been investigated. However each has limitations and disadvantages. Adsorption involves only phase transfer of pollutants without degradation; chemical oxidation is unable to mineralize all organic substances; and in biological treatment the slow reaction rates and the disposal of activated sludge are the drawbacks to be considered [27,28]. The photocatalytic process is highly promising because it operates at ambient temperature and pressure with low energy photons ($\lambda < 388$ nm for anatase TiO_2), requires no expensive catalysts or chemical reagents (except O_2 in the ambient air), and utilizes natural sunlight. Therefore, the photocatalytic method can be developed into a safe and economically viable remediating system [29].

Photocatalytic processes use light to generate conduction band (CB) electrons and valence band (VB) holes (e^- and

* Corresponding author. Tel.: +886 4 2219 6973; fax: +886 4 2219 4990.
E-mail address: cslu6@ntcnc.edu.tw (C.-S. Lu).

1010-6030/$ – see front matter © 2006 Elsevier B.V. All rights reserved.
doi:10.1016/j.jphotochem.2006.10.013

h^+) capable of initiating redox chemical reactions on semiconductors [30]. The VB holes are powerful oxidants that initiate the degradation reactions of a wide variety of organic compounds [31]. Many researchers have used different aqueous suspensions of semiconductor slurries irradiated by UV light to generate highly reactive intermediates, usually hydroxyl radical ($^{\bullet}$OH), that initiate a sequence of reactions leading to the partial or total destruction of organic pollutants such as chlorophenols, nitrogen-containing pesticides, and aromatic compounds [32–38]. Among the semiconductors used, titanium dioxide (TiO_2) is considered a very efficient catalyst that, unlike other semiconductors, is nontoxic, stable to photocorrosion, and low cost [39,40].

At present, no studies on MEK photocatalysis intermediates have been reported, and a detailed study of the photocatalytic degradation process might provide useful information for the use of TiO_2 in the treatment of MEK in aqueous solution. Therefore, this research focused on the identification of the reaction intermediates and understanding of the mechanistic details of the photodegradation of MEK in the TiO_2/UV light process as a foundation for future application of this energy saving technology.

2. Experimental

2.1. Materials and reagents

Michler's Ethyl Ketone (MEK) was obtained from Tokyo Kasei Kogyo Co. and used without any further purification. Sample solutions containing 10 mg L^{-1} of MEK in water were prepared, protected from light, and stored at 4 °C. HPLC analysis confirmed the presence of MEK as a pure organic compound. The TiO_2 nanoparticles (P25, ca. 80% anatase, 20% rutile; particle size, ca. 20–30 nm; BET area, ca. 55 m^2 g^{-1}) were supplied by Degussa Co. and used in all the photocatalytic experiments. Reagent-grade ammonium acetate and HPLC-grade methanol were purchased from Merck. De-ionized water was used throughout this study. The water was purified with a Milli-Q water ion-exchange system (Millipore Co.) to give a resistivity of 1.8×10^7 Ω cm.

2.2. Instruments

A Waters ZQ LC–MS system – equipped with a Waters 1525 Binary HPLC pump, a Waters 2996 Photodiode Array Detector, a Waters 717plus Autosampler, and a Waters micromass-ZQ4000 Detector – was used. An Empower software workstation was used for the LC–MS instrument control, data acquisition, and data processing. GC–MS analyses were run on a Perkin-Elmer AutoSystem-XL gas chromatograph interfaced to a TurboMass selective mass detector. The mineralization of the MEK was monitored by measuring the total organic carbon (TOC) content with a Dohrmann Phoenix 8000 Carbon Analyzer, which employs a u.v./persulfate oxidation method by directly injecting the aqueous solution. The reactor, a C-75 Chromato-Vue Cabinet of UVP, provides a wide area of illumination from the 15-W UV-365 nm tubes positioned on two sides of the cabinet interior.

2.3. Photodegradation experiments

An aqueous TiO_2 dispersion was prepared by adding 10 mg of TiO_2 powder to a 100 mL solution containing the MEK at appropriate concentrations. Prior to irradiation, the dispersions were magnetically stirred in the dark for ca. 30 min to ensure the establishment of an adsorption/desorption equilibrium. Irradiations were carried out using two UV-365 nm lamps (15 W). The distance between the irradiated solution and the lamps was 14 cm. An average irradiation intensity of 5.2 W/m^2 was maintained throughout the experiments and was measured by internal radiometer. At given irradiation time intervals, the dispersion was sampled, centrifuged, and subsequently filtered through a Millipore filter (pore size, 0.22 μm) to separate the TiO_2 particles.

2.4. Procedures and analyses

After each irradiation cycle, the amount of residual MEK was determined by HPLC. The analysis of organic intermediates was accomplished by HPLC-ESI-MS after readjustment of chromatographic conditions in order to make the mobile phase compatible with the working conditions of the mass spectrometer. Solvent A was 25 mM aqueous ammonium acetate buffer (pH 6.9), and solvent B was methanol. LC was carried out on an Atlantis^{TM} dC_{18} column (250 mm × 4.6 mm i.d., d_p = 5 μm). The mobile phase flow rate was 1.0 mL/min. A linear gradient was run as follows: $t = 0$, $A = 95$, $B = 5$; $t = 20$, $A = 50$, $B = 50$; $t = 35$–40, $A = 10$, $B = 90$; $t = 45$, $A = 95$, $B = 5$. The column effluent was introduced into the ESI source of the mass spectrometer. The quadruple mass spectrometer, equipped with an ESI interface with heated nebulizer probe at 350 °C, was used with an ion source temperature of 80 °C. ESI was carried out with the vaporizer at 350 °C, and nitrogen was used as sheath (80 psi) and auxiliary (20 psi) gas to assist with the preliminary nebulization and to initiate the ionization process. A discharge current of 5 μA was applied. Tube lens and capillary voltages were optimized for maximum response during the perfusion of the MEK standard.

Solid-phase extraction (SPE) was employed for preconcentration of irradiated samples prior to GC–MS analysis. Oasis HLB (hydrophilic/lipophilic balance) was used as the sorbent, and this ensures good recovery of compounds in a wide range of polarities. The cartridges were placed in a vacuum cube (provided by Supelco) and conditioned with 5 mL of methanol and 5 mL of deionized water. After the conditioning step, 1000 mL aliquots of the irradiated samples were loaded at a flow rate of approximately 10 mL/min. Elution was performed with 8 mL of methanol. The eluates obtained were concentrated by solvent evaporation with a gentle nitrogen stream and recomposed to a final volume of 1 mL in methanol. The extracts were stored in amber vials and refrigerated until chromatographic analysis to prevent further degradation.

GC–MS analyses were run on a Perkin-Elmer AutoSystem-XL gas chromatograph interfaced to a TurboMass selective mass detector. Separation was carried out in a DB-5 capillary column (5% diphenyl/95% dimethyl-siloxane), 60 m, 0.25-mm

i.d., and 1.0-μm thick film. A split–splitless injector was used under the following conditions: injection volume 1 μL, injector temperature 280 °C, split flow 10 mL/min. The helium carrier gas flow was 1 mL/min. The oven temperature program was 4.0 min at 40 °C, 4 °C/min to 80 °C (2 min), 8 °C/min to 280 °C (9 min). Typical MSD operating conditions were optimized by the autotuning software. Electron impact (EI) mass spectra were monitored from 35 to 300 *m/z*. The ion source and inlet line temperatures were set at 220 and 280 °C, respectively.

3. Results and discussion

3.1. Comparison of MEK degradation between photolysis and photocatalysis

To confirm the role of TiO_2 in the photocatalysis reaction, three sets of experiments were performed to compare MEK degradation rates with and without catalysts. One set was performed with MEK (10 mg L^{-1}) exposed to TiO_2 (100 mg L^{-1}) but no UV (a TiO_2 only condition). The second set was performed by exposing MEK (10 mg L^{-1}) to UV without TiO_2 (a photolysis condition). Then, the third set was performed by exposing MEK to TiO_2 (100 mg L^{-1}) in the presence of UV illumination (a photocatalysis condition). The results are presented in Fig. 1.

First, the experiment with TiO_2 showed that only a small amount of MEK (about 5%) was adsorbed on the TiO_2 surface. Control experiments performed in the dark indicated the hydrolysis and adsorption of MEK on TiO_2 particles did not affect its concentration during these experiments. Next, the results of the photolysis and photocatalytic experiments showed that the photolysis reaction resulted in a 79.7% decrease in the MEK concentration after 20 h while the MEK was 99.7% removed after 20 h in the case of the photocatalytic reaction. Fig. 1 clearly shows that on the initial stage the photocatalytic decomposition proceeds similar way to that in the absence of TiO_2. This shows that, up to 4 h, MEK absorbs UV light and blocks the irradiation for TiO_2. After the decomposition became $C/C_0 = 0.2$, the decomposition of MEK proceeds mainly by

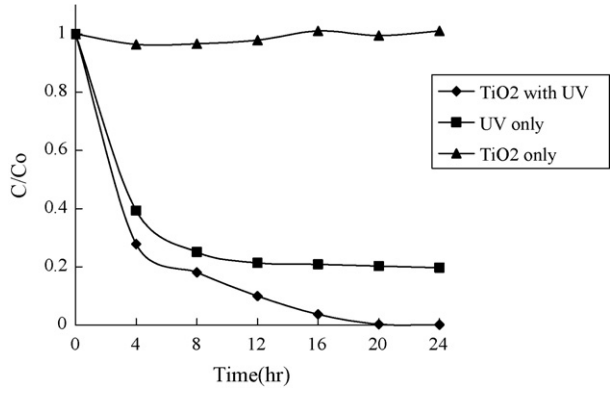

Fig. 1. MEK degradation under control conditions (TiO_2 only and UV only) and photocatalytic conditions (experimental conditions: MEK = 10 mg L^{-1}, TiO_2 = 0 mg L^{-1} in photolysis, 100 mg L^{-1} in photocatalysis, UV-365 nm = 5.2 W/m^2 in photolysis and photocatalysis conditions).

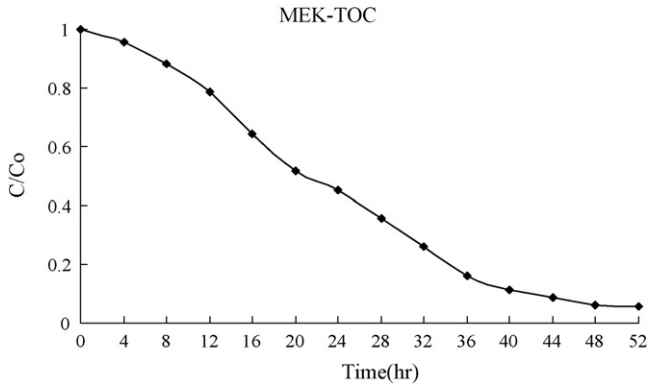

Fig. 2. Depletion in TOC measured as a function of irradiation time for an aqueous solution of MEK in the presence of TiO_2.

TiO_2 photocatalytic reaction. These results indicate that photocatalysis is more effective than direct photolysis for MEK degradation.

In order to confirm the mineralization during MEK photocatalysis, TOC measurement was performed. The results are shown in Fig. 2. It was found that more than 94% of the MEK was mineralized within 48 h by the photocatalytic reaction. The TOC data confirms that all of the organic compounds were mineralized when the TiO_2/UV process was applied to the MEK removal.

3.2. Identification of intermediates

A survey through the literature of studies undertaken on the degradation of MEK reveals that no reaction mechanism has been reported and that very little is known about the use of TiO_2 in the treatment of MEK in aqueous solution. A relatively low intensity UV-365 lamp (15 W) was used in this study for the identification of organic intermediates. This enabled us to obtain slower degradation rates and provide favorable conditions for the determination of photoproducts. Additionally, the initial MEK concentration (10 mg L^{-1}) was selected to be high enough to facilitate the identification of intermediate products.

Various approaches to the study of intermediates can be taken. Among the most effective are those based on the GC–MS and LC–MS techniques [41–43]. To get a better understanding of the mechanistic details of this TiO_2-assisted photodegradation of MEK with UV light irradiation, 19 intermediates of the process were identified and examined by the HPLC-ESI-MS and GC–MS techniques in this research. Fig. 3(a) displays a typical HPLC chromatogram of the reacted solution during irradiation in the presence of TiO_2. The solution consisted of 14 primary components at retention times of less than 45 min. One of the peaks was the initial MEK (peak 1); the other 13 (new) peaks are those of the intermediates formed. We denoted the MEK and its related intermediates as compounds 1–9 and 1′–4′. Except for the initial MEK, the other peaks increased at first and subsequently decreased, indicating formation and subsequent transformation of the intermediates. Fig. 3(b) shows the GC–MS chromatogram obtained for a SPE extract of MEK solution after 24 h of irradiation. Up to six compounds could be detected as possible

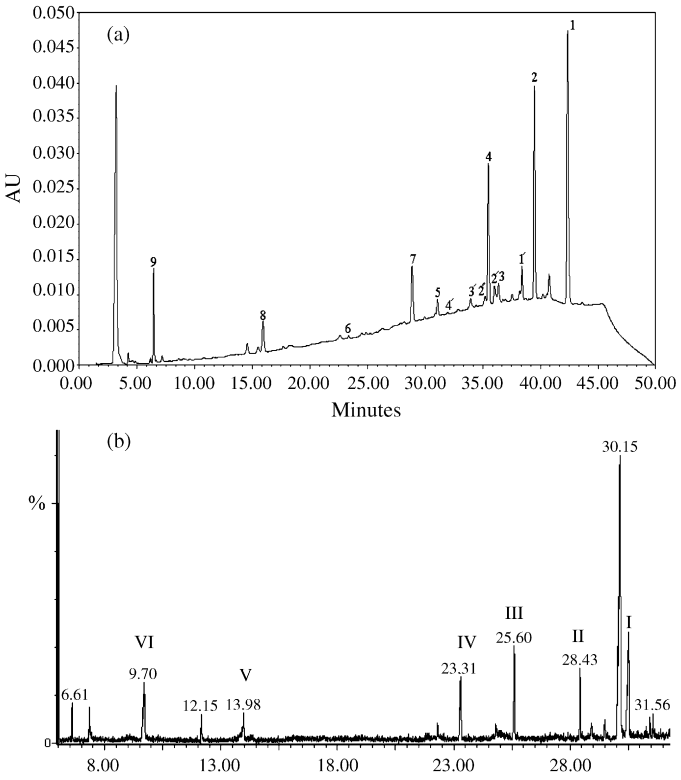

Fig. 3. (a) HPLC chromatogram of the photodegradation intermediates at 8 h of irradiation, recorded at 254 nm. (b) GC–MS/EI chromatogram obtained for a SPE extract of MEK solution after 24 h of irradiation with UV light in the presence of TiO_2 (100 mg L^{-1}).

degradation intermediates. We denoted these intermediates as compounds I–VI. Table 1 presents the retention times and the fragmentation patterns of the intermediates and the corresponding compounds identified by interpretation of their MS spectra.

From these results, several families of intermediates can be distinguished:

- The first one arises from the de-ethylation of 4-(*N*,*N*-diethylamino)-4′-(*N*′,*N*′-diethylamino)benzophenone (MEK) and includes compounds 2–6.
- The second family of intermediates (compounds 1′–4′) comes from the hydroxylation of the MEK derivatives.
- The third family of intermediates consist of compounds 7–9 formed by cleavage of the MEK derivatives, leading to aminobenzoic acid derivatives.
- The fourth family of intermediates (compounds I–III) detected by GC–MS is the result of the cleavage of the MEK derivatives, leading to aminobenzene derivatives.
- The last family of intermediates detected by GC–MS consist of compounds IV–VI formed by cleavage of the aromatic derivatives, leading to aliphatic products.

3.2.1. LC–MS determination

It is likely that the volatilities of several intermediates (compounds 1–9, and 1′–4′) are too small to be eluted out under the gas chromatographic conditions used, and the polarity so great that they were eluted with the solvent phase in our HPLC analysis (see Table 1 for detail). These compounds were identified by interpretation of the mass spectra. The molecular ion peaks appeared in the acid forms of the intermediates. Compound 1 was identified as 4-(*N*,*N*-diethylamino)-4′-(*N*′,*N*′-diethylamino) benzophenone (MEK) and exhibited a protonated molecular ion peak at $m/z = 325$ and a fragment ion at $m/z = 176$, which corresponded to the main fragment of the *N*,*N*-diethylaminobenzoyl group. Compound 2 was identified as 4-(*N*,*N*-diethylamino)-4′-(*N*′-ethylamino)benzophenone (DEBP) and exhibited a protonated molecular ion peak at $m/z = 297$, which corresponded

Table 1
Identification of the intermediates from the photodegradation of MEK by HPLC-ESI-MS and GC–MS

Peaks	Photodegradation intermediates	Abbreviation	RT (min)	MS peaks (*m*/*z*)
1	4-(*N*,*N*-Diethylamino)-4′-(*N*′,*N*′-diethylamino) benzophenone	DDBP (MEK)	42.66[a]	325, 176
2	4-(*N*,*N*-Diethylamino)-4′-(*N*′-ethylamino) benzophenone	DEBP	39.73[a]	297, 176, 148
3	4-(*N*-Ethylamino)-4-(*N*′-ethylamino) benzophenone	EEBP	36.63[a]	269, 148
4	4-(*N*,*N*-Diethylamino)-4′-aminobenzophenone	DBP	35.74[a]	269, 176, 120
5	4-(*N*-Ethylamino)-4′-aminobenzophenone	EBP	31.44[a]	241, 148, 120
6	4,4′-Bis-aminobenzophenone	BP	23.52[a]	213, 120
7	4-(*N*,*N*-Diethylamino)benzoic acid	DBAc	29.19[a]	194, 150
8	4-(*N*-Ethylamino)benzoic acid	EBAc	15.91[a]	166
9	4-Aminobenzoic acid	BAc	6.25[a]	138
1′	4-(*N*,*N*-Diethylamino)-4′-(*N*′-hydroxyethyl-*N*′-ethylamino)benzophenone	DHEBP	38.65[a]	341, 192, 176
2′	4-(*N*-Hydroxyethyl-*N*-ethylamino)-4′-(*N*′-ethyl amino)benzophenone	HEEBP	36.25[a]	313, 148
2″	4-(*N*,*N*-Diethylamino)-4′-(*N*′-hydroxyethyl amino)benzophenone	DHBP	35.48[a]	313, 176, 164
3′	4-(*N*-Ethylamino)-4′-(*N*′-hydroxyethylamino) benzophenone	EHBP	34.25[a]	285, 164, 148
4′	4-(*N*-Hydroxyethyl-*N*-ethylamino)-4′-amino benzophenone	HEBP	32.28[a]	285, 120
I	*N*,*N*-Diethylaminobenzene	DBz	30.52[b]	149, 134, 106, 77, 51
II	*N*-Ethylaminobenzene	EBz	28.43[b]	121, 106, 77
III	Aminobenzene	Bz	25.60[b]	93, 66, 39
IV	Acetamide	AAm	23.31[b]	59, 44, 43
V	2-Propenoic acid	PAc	13.98[b]	72, 55, 45, 27
VI	Acetic acid	AAc	9.70[b]	60, 45, 43

[a] The intermediates were identified by HPLC-ESI-MS.
[b] The intermediates were identified by GC–MS.

to the loss of one ethyl group from MEK. It also exhibited fragment ions at $m/z = 176$ and 148 which corresponded to the main fragments of the *N*,*N*-diethylaminobenzoyl and *N*-ethylaminobenzoyl groups, respectively.

Two species had protonated molecules of $m/z = 269$ eluted at retention times of 35.74 min (compound 4) and 36.63 min (compound 3) during LC–MS, suggesting the formation of di-*N*-de-ethylated products of MEK. Both intermediates display similar HPLC-ESI-MS characteristics. The intermediates were identified by interpretation of their fragment ions in the mass spectra. Compound 3 was identified as 4-(*N*-ethylamino)-4′-(*N*′-ethylamino)benzophenone (EEBP) and exhibited a protonated molecular ion peak at $m/z = 269$ and a fragment ion at $m/z = 148$ which corresponded to the main fragment of the *N*-ethylaminobenzoyl group. Compound 4 was identified as 4-(*N*,*N*-diethylamino)-4′-aminobenzophenone (DBP) and exhibited a protonated molecular ion peak at $m/z = 269$ and a fragment ions at $m/z = 176$ and 120 which corresponded to the main fragments of the *N*,*N*-diethylaminobenzoyl and 4-aminobenzoyl groups, respectively. The LC–MS chromatogram revealed a shorter retention time for compound 4 than for compound 3, suggesting compound 4 was more polar. Considering that the polarity of the DBP species exceeds that of the EEBP intermediate, we expected the latter to be eluted after the DBP species.

Compound 5 was identified as 4-(*N*-ethylamino)-4′-aminobenzophenone (EBP) and exhibited a protonated molecular ion peak at $m/z = 241$ which corresponded to the loss of three ethyl groups from MEK and fragment ions at $m/z = 148$ and 120 which corresponded to the main fragments of the *N*-ethylaminobenzoyl and 4-aminobenzoyl groups, respectively. Compound 6 was identified as 4,4′-bis-aminobenzophenone (BP) andexhibited a protonated molecular ion peak at $m/z = 213$ which corresponded to the loss of four ethyl groups from MEK and a fragment ion at $m/z = 120$ which corresponded to the main fragment of the 4-aminobenzoyl group. From the results of mass spectral analysis, we also confirmed that compounds 7–9, molecular ion peaks at $m/z = 194$, 166, and 138, in the liquid chromatogram were 4-(*N*,*N*-diethylamino) benzoic acid, 4-(*N*-ethylamino)benzoic acid, and 4-aminobenzoic acid, respectively.

The hydroxyethylated intermediates (1′–4′) did appear but seem to be unstable; they were observed at a lower concentration. Compound 1′ was identified as 4-(*N*,*N*-diethylamino)-4′-(*N*′-hydroxyethyl-*N*′-ethylamino) benzophenone (DHEBP) and exhibited a protonated molecular ion peak at $m/z = 341$ which corresponded to the addition of one hydroxyl group to MEK and fragment ions at $m/z = 192$ and 176 which corresponded to the main fragments of the *N*-hydroxyethyl-*N*-ethylaminobenzoyl and *N*,*N*-diethylaminobenzoyl groups, respectively. Two species had protonated molecules of $m/z = 313$ eluted at retention times of 35.48 min (compound 2″) and 36.25 min (compound 2′) during LC–MS analysis. The intermediates were identified by interpretation of their fragment ions in the mass spectra. Compound 2′ was identified as 4-(*N*-hydroxyethyl-*N*-ethylamino)-4′-(*N*′-ethylamino) benzophenone (HEEBP) and exhibited a protonated molecular ion peak at $m/z = 313$ which corresponded to the addition of one hydroxyl group to the *N*,*N*-diethylamino group of DEBP. It also exhibited a fragment ion at $m/z = 148$ which corresponded to the main fragment of the *N*-ethylaminobenzoyl group. Compound 2″ was identified as 4-(*N*,*N*-diethylamino)-4′-(*N*′-hydroxyethylamino)benzophenone (DHBP). It exhibited a protonated molecular ion peak at $m/z = 313$ which corresponded to the addition of one hydroxyl group to the *N*′-ethylamino group of DEBP. Also exhibited were fragment ions at $m/z = 176$ and 164 corresponding to the main fragments of the *N*,*N*-diethylaminobenzoyl and *N*-hydroxyethylaminobenzoyl groups, respectively.

Two species had protonated molecules of $m/z = 285$ eluted at retention times of 32.28 min (compound 4′) and 34.25 min (compound 3′) during LC–MS analysis. The intermediates were identified by interpretation of their fragment ions in the mass spectra. Compound 3′ was identified as 4-(*N*-ethylamino)-4′-(*N*′-hydroxyethylamino)benzophenone (EHBP). It exhibited a protonated molecular ion peak at $m/z = 285$ corresponding to the addition of one hydroxyl group to the *N*′-ethylamino group of EEBP and fragment ions at $m/z = 164$ and 148 which corresponded to the main fragments of the *N*-hydroxyethylaminobenzoyl and *N*-ethylaminobenzoyl groups, respectively. Compound 4′ was identified as 4-(*N*-hydroxyethyl-*N*-ethylamino) -4′-amino benzophenone (HEBP). It exhibited a protonated molecular ion peak at $m/z = 285$ which corresponded to the addition of one hydroxyl group to the *N*,*N*-diethylamino group of DBP and exhibited a fragment ion at $m/z = 120$ which corresponded to the main fragment of the 4-aminobenzoyl group.

3.2.2. GC–MS determination

The identification of intermediates was also performed by SPE followed by GC–MS analysis in EI mode. SPE has been demonstrated to be more efficient than traditional liquid–liquid extraction (LLE) in the analysis of water samples containing very polar intermediates resulting from the photocatalytic degradation process [44]. The GC–MS analysis of the irradiated mixture of MEK/TiO_2 solution showed the formation of several intermediate products. Out of these, six products have been identified by using an identification program of the NIST library with a fit value higher than 70% in all cases. The retention times and mass peaks of these intermediates I–VI are given in Table 1. The peaks eluting at 30.52, 28.43, 25.60, 23.31, 13.98 and 9.70 min during GC–MS were identified as *N*,*N*-diethylaminobenzene, *N*-ethylaminobenzene, aminobenzene, acetamide, 2-propenoic acid, and acetic acid with fit values of 88%, 78%, 84%, 70%, 87% and 96%, respectively, found by searching the mass spectra library. The former intermediates (compounds I–III) detected by GC–MS are the results of the cleavage of the MEK derivatives (compounds 1–6), leading to aminobenzene derivatives. The latter intermediates detected by GC–MS consist of compounds IV–VI formed by cleavage of the aromatic derivatives, leading to aliphatic products.

3.2.3. UV–vis spectra

The absorption spectra of several intermediate products are measured and depicted in Fig. 4. They are identified as 1–6 (Fig. 4a) and 7–9 (Fig. 4b), corresponding to the

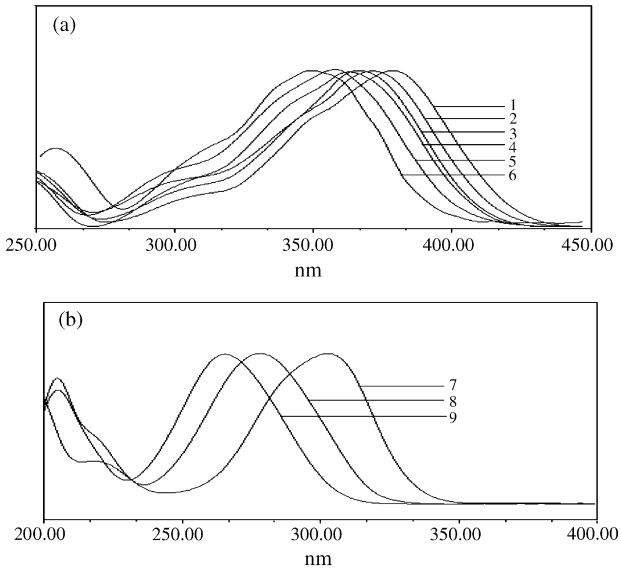

Fig. 4. Absorption spectra of *N*-de-ethylated intermediates formed during the photodegradation of MEK. Spectra were recorded using the photodiode array detector.

peaks 1–9 in Fig. 3(a), respectively. The absorption maximum of the spectral bands shifts hypsochromically from 379.5 nm (Fig. 4a, spectrum 1) to 342.6 nm (Fig. 4a, spectrum 6) and from 305.7 nm (Fig. 4b, spectrum 7) to 266.5 nm (Fig. 4b, spectrum 9). These hypsochromic shifts of the absorption bands are presumed to result from the formation of a series of *N*-de-ethylated intermediates in a stepwise manner. The *N*-de-ethylation of the 4-(*N*,*N*-diethylamino)-4′-(*N*′*N*′-diethylamino)benzophenone (MEK) has the wavelength position of its major absorption band moved toward the blue region, λ_{max}, MEK, 379.5 nm; DEBP, 373.5 nm; EEBP, 366.3 nm; DBP, 363.9 nm; EBP, 354.6 nm; BP, 342.6 nm. As well, to the extent that two *N*-ethyl groups are stronger auxochromic moieties than the *N*,*N*-diethyl or amino groups, the maximal absorption of the DBP intermediate was anticipated to occur at a wavelength shorter than the band position of the EEBP species. Similar phenomena were also observed during the photodegradation of sulforhodamine-B [45] and rhodamine-B [46] under visible irradiation. Moreover, in Fig. 4b, the hypsochromic shift of the absorption band is surmised to result from the formation of a series of aminobenzoic acid derivatives in a stepwise manner. The *N*-de-ethylation of the 4-(*N*,*N*-diethyl amino)benzoic acid (DBAc) has the wavelength position of its major absorption band moved toward the blue region, λ_{max}, DBAc, 305.7 nm; EBAc, 279.5 nm; BAc, 266.5 nm.

3.2.4. Evolution of intermediates

The relative distribution of several of the intermediate products (compounds 2–9 and 1′–4′) obtained is illustrated in Fig. 5. To minimize errors, the relative intensities were recorded at the maximum absorption wavelength for each intermediate. This was done even though the complete quantitative determination of all of the photogenerated intermediates was not achieved, owing to the lack of both appropriate molar extinction coefficients for these intermediates and reference standards. Nonetheless, we

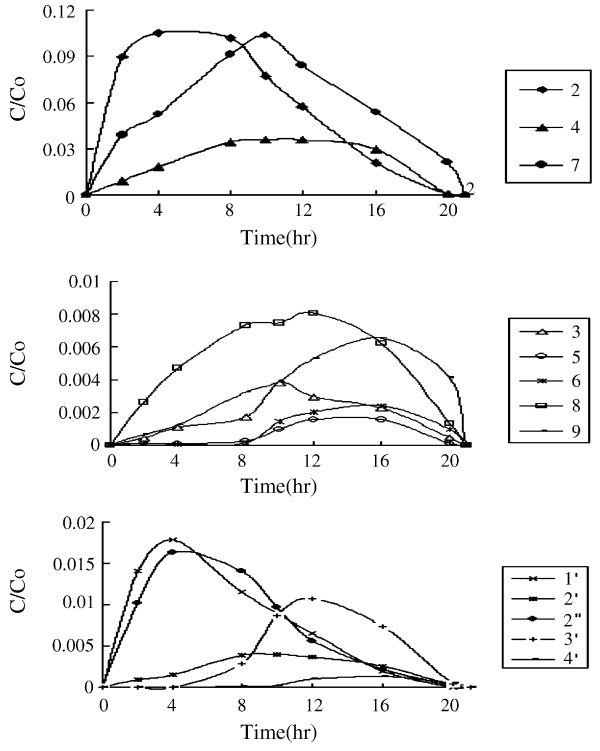

Fig. 5. Variation in the relative distribution of the intermediate products obtained from the photocatalytic degradation of MEK as a function of irradiation time. Curves 2–9 and 1′–4′ correspond to the peaks 2–9 and 1′–4′ in Fig. 3, respectively.

clearly observed the changes in the distribution of each intermediate during the photodegradation of MEK. The first product (DEBP) of *N*-de-ethylation reached its maximum concentration after a 4-h irradiation period (Fig. 5, curve 2). The *N*-di-de-ethylated intermediates (EEBP and DBP) were clearly observed (Fig. 5, curves 3 and 4) to reach their maximum concentrations after 10-h irradiation periods. The *N*-tri-de-ethylated intermediate (EBP) was clearly observed (Fig. 5, curve 5) to reach its maximum concentration after a 16-h irradiation period. The final *N*-de-ethylated intermediate (BP) was clearly observed (Fig. 5, curve 6) to reach its maximum concentration after a 16-h irradiation period. The successive appearance of the maximal quantity of each intermediate indicates that the *N*-de-ethylation of MEK is a stepwise photochemical process.

In the hydroxylation of the *N*-tetra-ethylated intermediate, (Fig. 5, curve 1′), DHEBP reached its maximum concentration after a 4-h irradiation period because the •OH attacked the *N*,*N*-diethyl group of MEK. In the hydroxylation of the *N*-tri-ethylated intermediates, (Fig. 5, curves 2′ and 2″), HEEBP and DHBP reached their maximum concentrations after 8- and 4-h irradiation periods because the •OH attacked the *N*,*N*-diethyl group of DEBP and the *N*-ethyl group of DEBP. Considering that the *N*,*N*-diethyl group is bulkier than the *N*-ethyl group in DEBP molecules, nucleophilic attack by •OH on the *N*-ethyl group should be favored at the expense of the *N*,*N*-diethyl group. In accord with this notion, the HPLC results showed that the DHBP intermediate reached maximal concentration before the HEEBP intermediate did. In the hydroxylation of *N*-di-ethylated

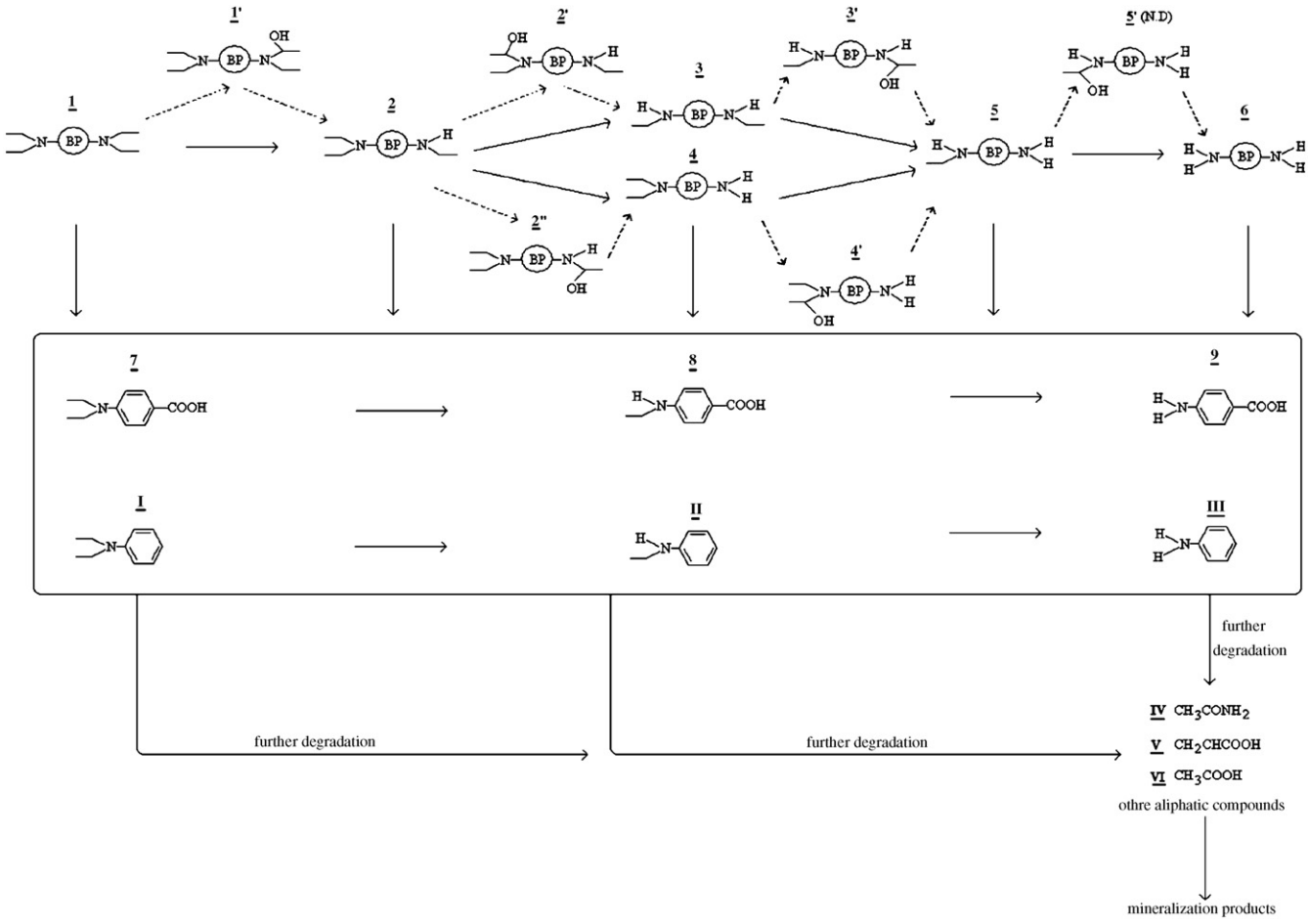

Scheme 1. Proposed photodegradation mechanism of the MEK under UV illumination in aqueous TiO_2 dispersions followed by the identification of several intermediates by HPLC-ESI-MS and GC–MS techniques.

intermediates, (Fig. 5, curves 3′ and 4′), EHBP and HEBP reached their maximum concentration after 12- and 16-h irradiation periods because the •OH attacked the *N*-ethyl group of EEBP and the *N*,*N*-diethyl group of DBP. The successive appearance of the maximal quantity of each intermediate indicates that the *N*-de-ethylation of MEK is a stepwise photochemical process that proceeds by a dehydroxylation of *N*-hydroxyethylated intermediates. We also analyzed the evolution of the photolysis degradation products by plotting areas of the corresponding LC peaks as functions of irradiation time. In the photolysis reaction, only trace amounts of the organic intermediates were produced, as shown in Fig. 6. Another difference in the production pattern between photolysis and photocatalysis is that the concentration of intermediates did not decrease, but increased steadily after 28 h of photolysis. The results we discussed above can be seen more clearly from Scheme 1.

3.3. Initial photooxidation pathway

Most aromatic molecules undergo photocatalytic degradation when irradiated in the presence of suitable semiconductors. This occurs through a multistep process involving the attack of the substrate by radical species, among which the •OH radical was recognized to be the most powerful oxidant [47]. Nakamura and Nakato [48] proposed a mechanism of water oxidation by a nucleophilic attack to a surface-trapped hole at a bridged O site. Murakami et al. [49] reported when the O–O bond in Ti–O–OH breaks the hydroxyl radicals can be formed from the bridge OH groups:

$$[\mathrm{Ti{-}O{-}Ti}]_s + h^+ + H_2O \rightarrow [\mathrm{Ti{-}O^{\bullet}HO{-}Ti}]_s + H^+$$

$$[\mathrm{Ti{-}O^{\bullet}HO{-}Ti}]_s \rightarrow [\mathrm{Ti{-}O{-}O{-}Ti}]_s + H^+$$

$$[\mathrm{Ti{-}O{-}O{-}Ti}]_s + H_2O \rightarrow [\mathrm{Ti{-}O{-}OH^{\bullet}HO{-}Ti}]_s$$

$$[\mathrm{Ti{-}O{-}OH^{\bullet}HO{-}Ti}]_s \rightarrow [\mathrm{Ti{-}O^{\bullet}HO{-}Ti}]_s + {}^{\bullet}OH$$

The great number of compounds detected during the degradation of MEK shows the complexity of the photocatalytic process and suggests the existence of various degradation routes resulting in multi-step and interconnected pathways. Scheme 1 shows the proposed mechanism behind the generation of the primary detected intermediates. It involves two different pathways (routes A and B, respectively), corresponding to the two possible sites for the attack of the •OH radicals on the MEK molecule.

The *N*-de-ethylation of the MEK occurs mostly by the attack of the •OH species on the *N*,*N*-diethyl groups of the MEK. The sequential reactions in the de-ethylation process (route A) are

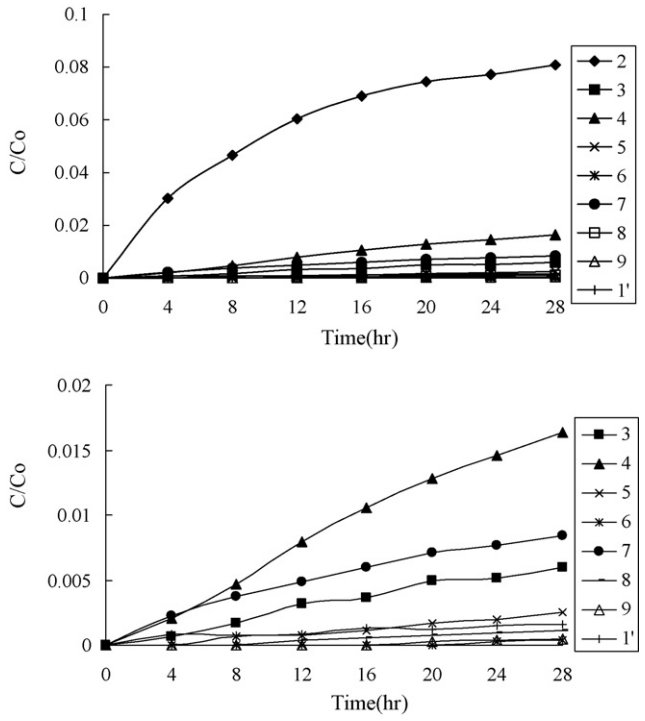

Fig. 6. Variation in the relative distribution of the intermediate products obtained from the photolysis degradation of MEK as a function of irradiation time. Curves 2–9 and 1′ correspond to the peaks 2–9 and 1′ in Fig. 3, respectively.

shown in Scheme 2. It is well known that the •OH radical is an electrophile and that C–H bonds adjacent to nitrogen are responsible for a pronounced stereoelectronic effect that produces high rates of H-atom abstraction. Therefore, the α-hydrogen atoms in the ethyl group of MEK molecule are the most prone to radical attack.

Hydroxyl radicals yield carbon-centered radicals upon the H-atom abstraction from the ethyl group, or they react with the lone-pair electron on the N atom to generate cationic radicals, which subsequently convert into carbon-centered radicals [24]. The carbon-centered radicals react rapidly with O_2 to produce peroxy radicals that subsequently transform into alkoxy radicals or into *N*-hydroxyethylated intermediates through the bimolecular Russell mechanism [50]. The fragmentation of the alkoxy radical produces a de-ethylated product. The mono-de-ethylated species, DEBP, can also be excited by UV light and be implicated in other similar events (H-atom abstraction, oxygen attack, and the bimolecular Russell mechanism) to yield the bi-de-ethylated intermediates, EEBP and DBP. The de-ethylation process as described above continues until formation of the completely de-ethylated species, BP.

In addition to the de-ethylation degradation route, an alternative pathway was also identified. A plausible mechanism (route B) for the formation of degradation products 7–9 and I–III involving electron transfer reactions and reaction with hydroxyl radicals formed in the photocatalytic system is proposed in

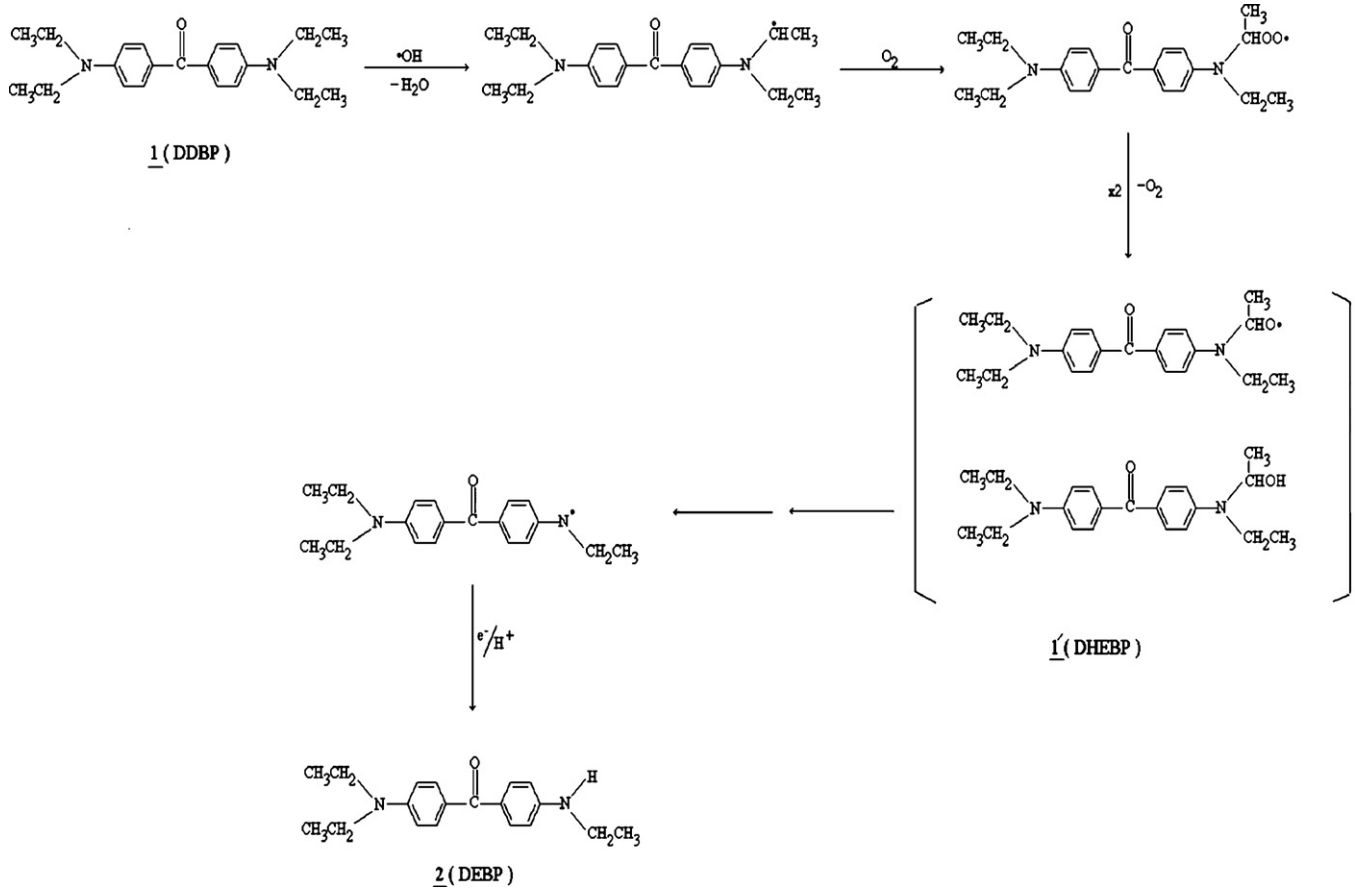

Scheme 2. Proposed pathways of photocatalytic degradation of MEK: route A.

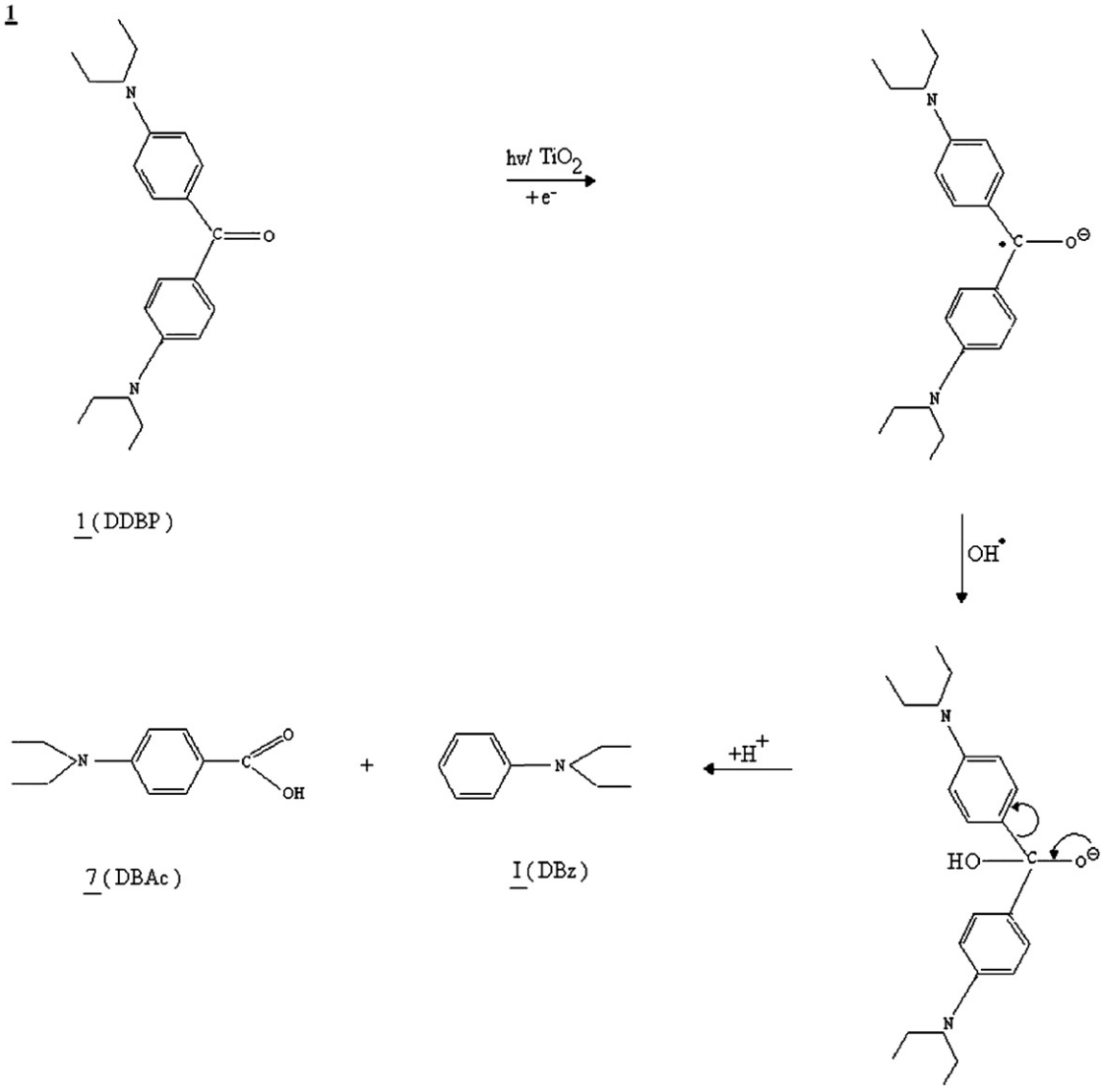

Scheme 3. Proposed pathways of photocatalytic degradation of MEK: route B.

Scheme 3. Upon the transfer of an electron the *N*-ethylated diaminobenzophenone derivatives (compounds 1–6) can form the radical anion, which can undergo the addition of a hydroxyl radical and form the anionic species, which upon cleavage can lead to the formation of aminobenzoic acid derivatives (compounds 7–9) and aminobenzene derivatives (compounds I–III).

It is known from previous photocatalytic studies that, after the formation of various aromatic derivatives, cleavage of the benzene or other organic rings takes place, and different aliphatic products are subsequently formed before complete mineralization [47]. Even though further oxidation leads to the ring-opening and the formation of aliphatic oxidation derivatives (compounds IV–VI), these species will not be discussed here.

4. Conclusion

The photocatalytic degradation of the MEK is a fast process and includes the formation of several intermediates that were identified using GC–MS and LC–MS techniques. The percentage decreases in MEK concentration, resulting from the photolysis and photocatalytic reactions conducted for 20 h, were 79.7% and 99.7%, respectively. The TOC data shows that eventually all the organic compounds (>94%) are mineralized within 48 h by the photocatalytic reaction. Nineteen intermediates have been identified and characterized through a mass spectra analysis, giving insight into the early steps of the degradation process. The results reported here show that the combination of GC–MS with EI and LC–MS with electrospray ionization represents a powerful analytical approach to the confirmation of the molecular structure of photocatalytic intermediates.

The photocatalytic degradation of MEK proceeds through competitive reactions such as *N*-de-ethylation and destruction of the bis-aminobenzophenone structure. The former path generates a carbon-centered radical upon H-atom abstraction, which further reacts with O_2 generating peroxy and alkoxy radical intermediates to result in a series of *N*-hydroxyethylated and *N*-de-ethylated products. The hypsochromic effects resulting from *N*-de-ethylated intermediates of MEK occurred

concomitantly during irradiation. In the latter path, the electron in the conduction band of TiO_2 can be picked up by the adsorbed MEK derivatives, leading to the formation of radical anion, which can undergo addition of a hydroxyl radical forming the anionic species, which upon cleavage can lead to the formation of aminobenzoic acid derivatives and aminobenzene derivatives. The reaction mechanisms of TiO_2/UV proposed in this research should prove useful in future efforts to breakdown the organic compounds in wastewater.

References

[1] L. Castle, A.P. Damant, C.A. Honeybone, S.M. Johns, S.M. Jickells, M. Sharman, J. Gilbert, Food Addit. Contam. 14 (1997) 45–52.
[2] A. Ozaki, Y. Yamaguchi, T. Fujita, K. Kuroda, G. Endo, Food Chem. Toxicol. 42 (2004) 1323–1337.
[3] S.J.T. Pollard, G.D. Fowler, C.J. Sollars, R. Perry, Sci. Total Environ. 116 (1992) 31–52.
[4] K. Banerjee, P.N. Cheremisinoff, S.L. Cheng, Environ. Sci. Technol. 29 (1995) 2243–2251.
[5] G.J. O'Brien, Water Environ. Res. 64 (1992) 877–883.
[6] G. Mascolo, A. Lopez, R. Foldenyi, R. Passino, G. Tiravanti, Environ. Sci. Technol. 29 (1995) 2987–2991.
[7] R.M. Wittich, Appl. Microbiol. Biotechnol. 49 (1998) 489–499.
[8] H. Ballerstedt, A. Kraus, U. Lechner, Environ. Sci. Technol. 31 (1997) 1749–1753.
[9] A.D. Konstantinov, A.M. Johnston, B.J. Cox, J.R. Petrulis, M.T. Orzechowski, N.J. Bunce, C.H.M. Tashiro, B.G. Chittim, Environ. Sci. Technol. 34 (2000) 143–148.
[10] Z. Qin, Chemosphere 33 (1996) 91–97.
[11] M.P. Colombini, F.D. Francesco, R. Fuoco, Microchem. J. 54 (1996) 331–337.
[12] K.J. Friesen, M.M. Foga, M.D. Loewen, Environ. Sci. Technol. 30 (1996) 2504–2510.
[13] M.H. Dung, P.W. O'Keefe, Environ. Sci. Technol. 28 (1994) 549–554.
[14] K.J. Friesen, D.C.G. Muir, G.R.B. Webster, Environ. Sci. Technol. 24 (1990) 1739–1744.
[15] S. Kieatiwong, L.V. Nguyen, V.R. Herbert, M. Hackett, G.C. Miller, M.J. Miille, R. Mitzel, Environ. Sci. Technol. 24 (1990) 1575–1580.
[16] D. Dulin, H. Drossman, T. Mill, Environ. Sci. Technol. 20 (1986) 72–77.
[17] A.J. Dobbs, C. Grant, Nature 278 (1979) 163–164.
[18] I.K. Konstantinou, T.A. Albanis, Appl. Catal. B: Environ. 49 (2004) 1–14.
[19] N. Watanabe, S. Horikoshi, H. Kawabe, Y. Sugie, J. Zhao, H. Hidaka, Chemosphere 52 (2003) 851–859.
[20] V.N. Kouloumbos, D.F. Tsipi, A.E. Hiskia, D. Nikolic, R.B. Breemen, J. Am. Soc. Mass Spectrom. 14 (2003) 803–817.
[21] I. Liu, L.A. Lawton, P.K.J. Robertson, Environ. Sci. Technol. 37 (2003) 3214–3219.
[22] C. Chen, P. Lei, H. Ji, W. Ma, J. Zhao, H. Hidaka, N. Serpone, Environ. Sci. Technol. 38 (2004) 329–337.
[23] N. Daneshvar, M. Rabbani, N. Modirshahla, M.A. Behnajady, J. Photochem. Photobiol. A: Chem. 168 (2004) 39–45.
[24] J. Lee, W. Choi, Environ. Sci. Technol. 38 (2004) 4026–4033.
[25] C.C. Chen, H.J. Fan, C.Y. Jang, J.L. Jan, H.D. Lin, C.S. Lu, J. Photochem. Photobiol. A: Chem. 184 (2006) 147–154.
[26] C.C. Chen, C.S. Lu, Y.C. Chung, J. Photochem. Photobiol. A: Chem. 181 (2006) 120–125.
[27] E. Pelizzetti, V. Maurino, C. Minero, V. Carlin, E. Pramauro, O. Zerbinati, M. Tosato, Environ. Sci. Technol. 24 (1990) 1565–1599.
[28] K.H. Wang, Y.H. Hsieh, M.Y. Chou, C.Y. Chang, Appl. Catal. B: Environ. 21 (1999) 1–8.
[29] W. Choi, S.J. Hong, Y.-S. Chang, Y. Cho, Environ. Sci. Technol. 34 (2000) 4810–4815.
[30] N. Serpone, E. Pelizzetti (Eds.), Photocatalysis-Fundamentals and Applications, Wiley–Interscience, New York, 1989.
[31] M.R. Hoffmann, S.T. Martin, W. Choi, D.W. Bahnemann, Chem. Rev. 95 (1995) 69–96.
[32] K.H. Wang, Y.H. Hsieh, M.Y. Chou, C.Y. Chang, Appl. Catal. B: Environ. 21 (1999) 1–8.
[33] I.K. Konstantinou, V.A. Sakkas, T.A. Albanis, Water Res. 36 (2002) 2733–2742.
[34] C. Richard, S. Bengana, Chemosphere 33 (1996) 635–641.
[35] W.Z. Tang, C.P. Huang, Water Res. 29 (1995) 745–756.
[36] J.P. Percherancier, R. Chapelon, B. Poyet, J. Photochem. Photobiol. A: Chem. 72 (1995) 261–266.
[37] A. Zaleska, J. Hupka, M. Wiergowski, M. Biziuk, J. Photochem. Photobiol. A: Chem. 135 (2000) 213–220.
[38] J.M. Hermann, J. Disdier, P. Pichat, S. Malato, J. Blanco, Appl. Catal. B: Environ. 17 (1998) 15–23.
[39] J.M. Hermann, C. Guillard, M. Arguello, A. Aguera, A. Tejedor, L. Piedra, A. Fernadez-Alba, Catal. Today 54 (1999) 353–367.
[40] I. Poulios, M. Kositzi, A. Kouras, J. Photochem. Photobiol. A: Chem. 115 (1998) 175–183.
[41] S. Chiron, A. Fernandez-Alba, A. Rodriguez, Trends Anal. Chem. 16 (1997) 518–527.
[42] S. Malato, J. Caceres, A.R. Fernandez-Alba, L. Piedra, M.D. Hernando, A. Aguera, J. Vial, Environ. Sci. Technol. 37 (2003) 2516–2524.
[43] C.C. Wong, W. Chu, Environ. Sci. Technol. 37 (2003) 2310–2316.
[44] A.R. Fernandez-Alba, A. Aguera, M. Contreras, G. Penuela, I. Ferrer, D. Barcelo, J. Chromatogr. A 823 (1998) 35–47.
[45] C. Chen, W. Zhao, J. Li, J. Zhao, H. Hidaka, N. Serpone, Environ. Sci. Technol. 36 (2002) 3604–3611.
[46] T. Wu, G. Liu, J. Zhao, H. Hidaka, N. Serpone, J. Phys. Chem. B 102 (1998) 5845–5851.
[47] P.A. Bianco, M. Vincenti, A. Banciotto, E. Pramauro, Appl. Catal. B: Environ. 22 (1999) 149–158.
[48] R. Nakamura, Y. Nakato, J. Am. Chem. Soc. 126 (2004) 1290–1298.
[49] Y. Murakami, E. Kenji, A.Y. Nosaka, Y. Nosaka, J. Phys. Chem. B: Lett., Published on Web 08/05/2006.
[50] G.A. Russell, J. Am. Chem. Soc. 79 (1957) 3871.